

Article

Design and Testing of an Automatic Strip-Till Machine for Conservation Tillage of Corn

Qi Wang¹, Bo Wang¹, Mingjun Sun², Xiaobo Sun¹ , Wenqi Zhou¹, Han Tang¹ and Jinwu Wang^{1,*} 

¹ College of Engineering, Northeast Agricultural University, Harbin 150030, China; wangqi@neau.edu.cn (Q.W.); s210702036@neau.edu.cn (B.W.); sunxiaobo@neau.edu.cn (X.S.); zwq@neau.edu.cn (W.Z.); tanghan@neau.edu.cn (H.T.)

² College of Agriculture, Northeast Agricultural University, Harbin 150030, China; a01210500@neau.edu.cn

* Correspondence: jinwuw@neau.edu.cn; Tel.: +86-0451-5519-0950

Abstract: Successive years of straw mulching and returning straw to the fields in Northeast China have made strip-tillage necessary, and reasonable strip-tillage operations can create conditions for crop growth. However, there are limited research studies on the related equipment applicable to this area. In this paper, an automatic control strip-tillage machine is designed. According to the conventional planting pattern of maize in this region, the operative processes of the machine were determined, and a suitable strip seedbed structure could then be constructed under straw mulching conditions. The type of coulters and the structural parameters of the V-type soil-crushing wheel were determined through theoretical analysis. Based on the air spring and electric linear actuator, the plowing depth control system and the straw width control system were developed, respectively, so as to improve the stability of the machine operation. Field tests showed that when the forward speed, tillage depth, and theoretical width were 6–12 km/h, 6–12 cm, and 18–24 cm, respectively, the straw clearing rate, soil crushing rate, and tillage depth and breadth stability were higher than 90%, and the soil flatness was less than 2 cm. All the indexes satisfied the agronomic and technological requirements of corn cultivation. The results of this study can provide equipment and technical support for the further popularization of conservation tillage technology.

Keywords: conservation agriculture; strip-tillage; straw residue management; automatic control technology; field test



Citation: Wang, Q.; Wang, B.; Sun, M.; Sun, X.; Zhou, W.; Tang, H.; Wang, J. Design and Testing of an Automatic Strip-Till Machine for Conservation Tillage of Corn.

Agronomy **2023**, *13*, 2357. <https://doi.org/10.3390/agronomy13092357>

Academic Editor: Andrea Peruzzi

Received: 19 August 2023

Revised: 4 September 2023

Accepted: 7 September 2023

Published: 11 September 2023



Copyright: © 2023 by the authors. Licensee MDPI, Basel, Switzerland. This article is an open access article distributed under the terms and conditions of the Creative Commons Attribution (CC BY) license (<https://creativecommons.org/licenses/by/4.0/>).

1. Introduction

Corn is one of the most significant cereal crops in China [1] with 30% of corn planted in the black land area of Northeast China [2,3], and its planting and production scales are crucial for food security [4]. The conservation tillage mode, based on returning straw to the land and no tillage, has been widely applied in Northeast China [5,6], and has alleviated the problems caused by traditional tillage, including topsoil thinning, decrease in soil organic matter, severe wind and water erosion, and haze due to straw burning [7–9]. This tillage mode has also efficiently improved food security and the eco-environment [10]. However, the straw residues can easily wrap around and block the planting machines and lead to a decrease in work efficiency. The residues could also reduce the consistency of the top soil and seeding quality, while the slow recovery of the ground temperature could affect seedling emergence and crop growth. All of these problems restrict the popularization of conservation agricultural technology [11–14].

Strip-tillage is a new conservation tillage technique that could effectively handle the problems inherent in returning straw to the land [7,15,16]. Strip-tillage creates a clean and consistent seedbed on the straw-covered surface and transfers the residue of the straw between the two strips to protect the soil. The seeds are planted in the cultivated strips [17]. Celik et al. [18], Godsey et al. [19], Alghamdi et al. [20], as well as Morrison and

Sanabria [21] determined that the plant residue retained between the strips reduces water evaporation in the soil, which has a significant impact on soil temperature and humidity, thus providing more favorable conditions for the initial stage of crop growth. Compared with conventional tillage, strip-tillage reduces the soil surface area disturbance by 50–75% and reduces the need for tractor operations, resulting in reduced energy input and higher crop yields at lower production costs [22–24].

The strip-tillage machine is a key piece of equipment for implementing strip-tillage technology [25,26]. Jia et al. have developed a 1GH-3 type inter-row tillage machine, which can realize the conversion of three operation modes (inter-row, ridge platform, and full-width rotary tillage) by disassembling and assembling the blades on the knife roller [27]. The active strip-tillage machine produced by Northwest Tillers in the United States can adapt to the cultivation requirements of different crops by adjusting the arrangement method of the rotary tillers. Due to the shortcomings of low work efficiency, high power consumption, and poor adaptability to different ridge distances, active strip-tillage machines have been basically phased out. At present, strip-tillage machines are mainly passive. Kristina Lekavičienė et al. built a passive strip-tillage machine using row cleaners and narrow tines and discs for soil loosening, and confirmed that the front angle of the ridging cutter had no significant effect on CO₂ emissions and diesel fuel consumption. Increasing the driving speed and depth of the plow blade has significant effects on diesel fuel consumption and the tractor's CO₂ emissions. Agricultural machinery manufacturing enterprises in Europe and the United States have successively launched passive products, such as the Sunflower 7610 (AGCO, Duluth, GA, USA) and the Kultistrip (Kverneland, Kerteminde, Denmark), which have achieved good operational results in the local area. At present, there are few reports on the overall design of passive strip-tillage machines in the existing research, and models produced in Europe and the United States have not been introduced to China. Therefore, there is a lack of machines suitable for the special working conditions in Northeast China.

The strip-tillage model and its supporting equipment have broad development prospects and market demand in China. Improving the work efficiency and quality of planters under straw-covered conditions has become an urgent issue. Therefore, in accordance with the agronomic requirements of corn conservation tillage and the technical requirements of planting operations in Northeast China, an automatic strip-till machine was developed. Each key working component was designed through theoretical analysis and electronic control technology, and the operating performance of the machine was verified through field tests. The research in this paper can provide a new research concept and method for the design of strip-till machines. At the same time, it can also promote conservation tillage in Northeastern China and slow down the rate of soil erosion of black soil resources in the region, which is of great ecological significance.

2. Materials and Methods

2.1. Overall Design of Automatic Strip-Till Machine

The design purpose of the strip-till machine was to build a high-quality seedbed with no straw residues and a consistent structure of the tillage layer prior to sowing. The structure of the constructed seedbeds is shown in Figure 1. Thus, the design requirements of the strip-till machine are as follows: (1) high-quality straw-cutting and strip-cleaning abilities, assuring clean ground after operation; (2) high soil-loosening and soil-crushing abilities, in order to create a suitable environment for planting operations and plant growth; (3) high ground profiling by the row units to ensure consistent tillage depth and promote seed germination.

In order to provide a theoretical reference for the design of the strip-till mechanism, the corn stubble in the field was measured, and the related physical parameters were counted. The row spacing of conventional ridges (D) was 65 cm; the maximum diameter of the underground root system (D_1) was 18 cm; the dense area of the underground root

system (H_1) was 0~6 cm; and the non-dense area of the underground root system (H_2) was 6~12 cm.

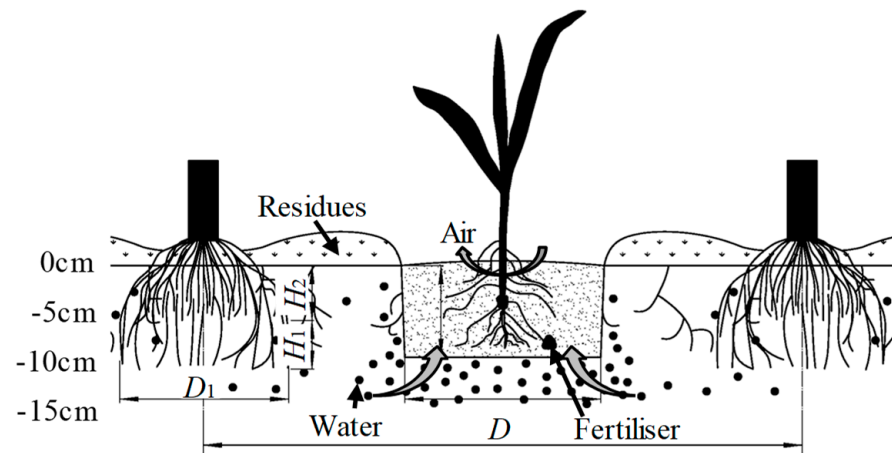


Figure 1. Schematic diagram of the seedbed structure constructed by strip-till machine.

2.1.1. Machine Construction

As shown in Figure 2, the overall structure of the automatic strip-till machine consisted of a frame assembly, control boxes, two strip-till units, a pneumatic transmission pipeline, and a ground wheel assembly. The strip-till unit consisted of a profiling mechanism, a tillage-depth-stabilization control system, a straw cutting coulters, an automatic-width-control row cleaner, two soil-loosening coulters, and a V-shaped soil-crushing wheel. The front of the frame assembly was welded with a three-point suspension bracket to connect with the tractor. The ground wheel assembly was installed on the front beam of the frame assembly and served as a spacing reference for the unit. The strip-till unit was fixed onto the rear beam of the frame assembly and moved along with the tractor. The control boxes were installed on the frame assembly, and equipped inside with a tillage-depth-stabilization control system and an automatic-width-control row-cleaning system. The air emitted from the tillage-depth-stabilization control system was transported via a pneumatic transmission pipeline to air springs, thereby offering downforce to the strip-till unit. The overall structure is shown in Figure 2. The main technical parameters are set out in Table 1.

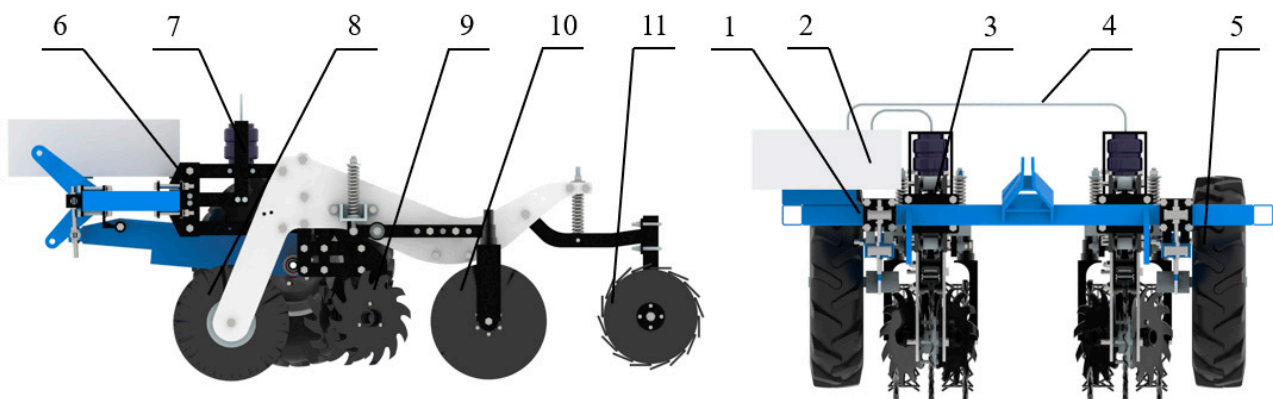


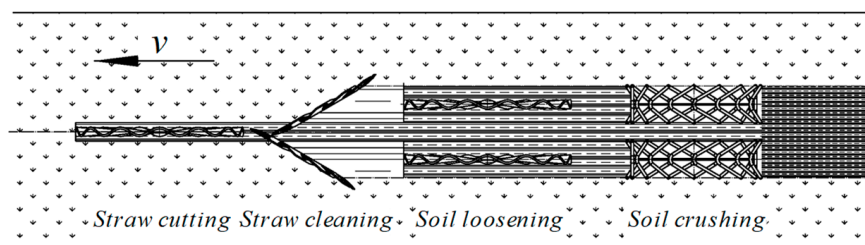
Figure 2. Structure sketch of the automatic strip-till machine: 1—frame assembly; 2—control boxes; 3—strip-till unit; 4—pneumatic transmission pipeline; 5—ground wheel assembly; 6—profiling mechanism; 7—tillage-depth-stabilization control system; 8—straw cutting coulters; 9—automatic-width-control row cleaner; 10—soil-loosening coulters; 11—V-shaped soil-crushing wheel.

Table 1. Main technical parameters.

Parameters	Values
Structure type	Three-point suspension
Dimension (length × width × height)/mm	1800 × 920 × 300
Machine quality (kg)	300
Row spacing (mm)	450–950
Working width (mm)	180–240
Tillage depth (mm)	60–120
Working speed (km·h ⁻¹)	6–12

2.1.2. Working Principle

The automatic strip-till machine adopted a combined operating mode. Before working, the tillage-depth-stabilization control system regulated the air pressure inside air springs according to actual working conditions and agronomic requirements, and provided the unit with appropriate downforce, so it reached and maintained the target tillage depth. A pressure threshold was set for the automatic-width control system, which ensured the automatic row cleaner could operate stably at a suitable width. The space between the soil-loosening coulters and the rotating arm length was adjusted to the working width of the strip-till unit. During operation, this machine cleaned strips and tilled straw-covered land in the order of straw cutting > straw cleaning > soil loosening > soil crushing. The coulters cut off the residual straw between rows, and the automatic-width row cleaner pushed the residual straws into the working row and threw them to the two sides of the working width. The soil-loosening coulters loosened and broke the soil under the preset width in a clean row. Following that, the V-shaped soil-crushing device impacted and broke the loosened soil, forming clean and consistent strips. The working principle of the machine is shown in Figure 3.

**Figure 3.** The working process of the machine.

2.2. Design of Key Components

2.2.1. Design of Soil-Loosening and Soil-Crushing Device

The main purpose of the strip-till machine is to standardize the loosening and crushing of the soil in the cultivation layer and build a high-quality seedbed. The realization of the machine is via a 3-coulter soil-loosening system to integrate with the initial loosening of the cultivation layer soil. Then, the V-shaped soil-crushing wheel is used to crush the loose soil again.

Coulters are the key working parts of the strip-till unit, and the rationality of their allocation optimization significantly affects the working quality and power consumption of the machine. The results of previous studies showed that there are significant differences in working resistance, soil disturbance area, and furrow widths among different types of coulters in the field tests. The cutting force, maximum furrow width, and furrow disturbance area of a notched-flat coulter (NF) are significantly lower than those of fluted coulters. Compared with an 8-wave fluted coulter (8 w), the cutting force of a 13-wave fluted coulter (13 w), 18-wave fluted coulter (18 w), and 25-wave fluted coulter (25 w) was reduced by 25.4%, 47.9%, and 52.7%; the maximum furrow width was reduced by 9.6%, 30.5%, and 24.0%; and the furrow disturbance area was reduced by 20.2%, 36.1%, and 22.8%,

respectively. Under the straw covering condition, the NF and large-wavenumber fluted coulters (18 w and 25 w) could cut straw residue at a low cutting force, and were more suitable for straw residue cutting. Under the condition of the ground not being covered with straw, the small-wavenumber fluted coulters (8 w and 13 w) could create furrows with a larger furrow width and disturbance area, and were more suitable for soil loosening and crushing [28].

The effect of the cutting force should also be considered during allocation optimization, as the formation of wide furrows requires a larger cutting force and consumes more power. In this paper, with comprehensive consideration of cutting force and furrow profiles, the 18 w coulters which was installed at the front of the row cleaner of the strip-till machine would be beneficial for cutting straw residue in fields, and the 13 w coulters which was installed at the back of the row cleaner was a more desirable tool for loosening soil without straw mulching. The 3-coulters soil-loosening system consists of the two types of coulters mentioned above, which were arranged at the front and back, achieving the initial loosening of the cultivation layer soil. Table 2 shows the main technical parameters of the two types of coulters.

Table 2. Main technical parameters of the two types of coulters.

Parameters	13 Waves-Fluted Coulters	18 Waves-Fluted Coulters
Diameter (mm)	406	406
Working width (mm)	25.5	12
Effective waves	3.82	5.29
Chamfer types	double-side	double-side

2.2.2. Design of V-Shaped Soil-Crushing Wheel

Crushing soil was the last process of the machine. A V-shaped soil-crushing wheel was designed, as shown in Figure 4. The V-shaped soil-crushing teeth arranged in a circle were used to crush the soil again after the loosening of the soil via the coulters operation, which can eliminate the over-large soil blockages in the working width and increase the breakage rate of the soil.

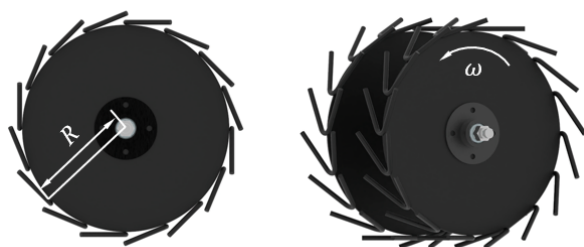


Figure 4. Structure sketch of the V-shaped soil-crushing wheel.

The design requirements of the V-shaped soil-crushing wheel are as follows: the soil-crushed pitch should be selected appropriately, as too large a pitch would reduce soil breakage rate, and too small a pitch would cause soil adhesion; the soil-crushed width should be slightly smaller than the working width of the soil-loosening coulters, in order to prevent the wheel working on uncultivated land and being unable to enter the soil. The number of soil-crushing teeth can be solved by Equation (1).

$$z = \frac{\pi R}{2\eta\lambda S} \quad (1)$$

where z is the number of soil-crushing teeth evenly distributed on the circumference; R is the wheel radius, mm; η is the slip rate; λ is the rotation speed ratio; and S is the soil-crushed pitch, mm.

According to the design requirements and Equation (1), the main parameters were determined, the soil-crushed pitch (S) was 80 mm, the rotation speed ratio (λ) was 1, the slip rate (η) was 0.8, the wheel radius (R) was 165 mm, and the number of soil-crushing teeth evenly distributed on the circumference (z) was 16.

2.2.3. Design of Automatic-Width Row Cleaner

The automatic row cleaner can construct a suitable working environment for the soil-loosening coulters. It was installed in front of the soil-loosening coulters to clean the residual straw in the seedbeds. An S-shaped pressure sensor and an electric linear actuator were used in concert to monitor and control the soil downforce and depth of the straw-cleaning wheels in real time, so that the working width was accurately controlled. As shown in Figure 5, it mainly consisted of a parallel four-link profiling frame, two star-tooth concave straw-cleaning wheels, and an automatic-width control system (an S-shaped pressure sensor, an electric linear actuator, a connecting piece, and a width control module). The S-shaped pressure sensor and the electric linear actuator were connected through the connecting piece to constitute a pressure detection and control unit whose two ends were attached to the two ends of the parallel four-link profiling frame.

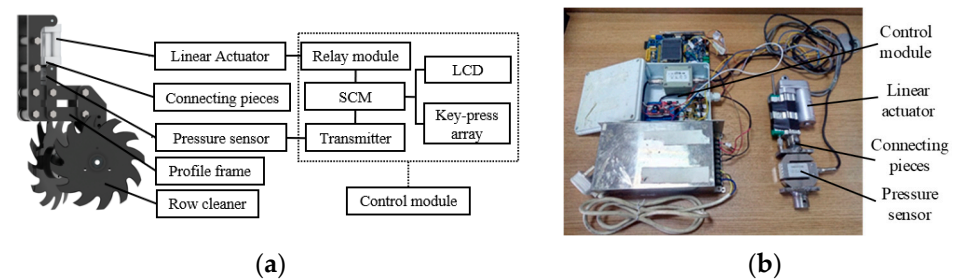


Figure 5. Structure sketch of the automatic row cleaner: (a) schematic diagram; (b) the automatic-width control system.

The star-tooth concave straw-cleaning wheels are the key part of the automatic row cleaner [29]. In order to increase the straw cleaning rate and avoid missing any areas, a staggered and opposite arrangement of the straw-cleaning wheels was adopted. The straw-cleaning wheels are shown in Figure 6. The main parameters are as follows: the radius (r) is 152.5 mm; the angle between the cleaning wheel and the advancing direction (α) is 30° ; the angle between the cleaning wheel and the vertical plane (β) is 15° ; and the distance between the two cleaning wheels (L) is 90 mm. When the working depth of the row cleaner is 20 mm, the straw cleaning width and the missed area are 225 mm and 0 mm, respectively, which meets the agronomic requirements.

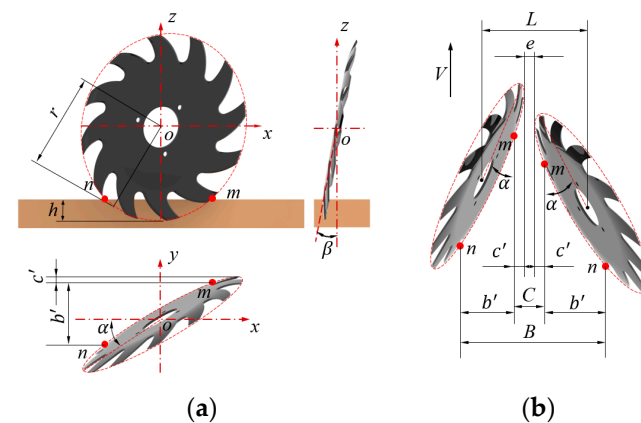


Figure 6. Schematic sketch of theoretical working width: (a) installation diagram; (b) sketch of theoretical working width.

The Oxyz coordinate system was established with the center of the straw-cleaning wheels as the coordinate origin, where the x -axis was the forward direction of the machine, the y -axis was the horizontal direction perpendicular to the forward direction of the machine, and the z -axis was the vertical direction. Then, the theoretical working width and the theoretical missed areas of the row cleaner can be expressed by Equation (2)

$$\begin{cases} B = 4\sqrt{r^2 - (r - h)^2} \sin \alpha + 2\left(r - \sqrt{r^2 - (r - h)^2}\right) \sin \alpha \\ \quad - 2(r - h) \sin \beta \cos \alpha + e \\ C = 2\left(r - \sqrt{r^2 - (r - h)^2}\right) \sin \alpha - 2(r - h) \sin \beta \cos \alpha + e \end{cases} \quad (2)$$

where B is the theoretical working width of the row cleaner, mm; C is the theoretical missed area of the row cleaner, mm; e is the horizontal distance of the intersection point between two straw-cleaning wheels, mm; r is the radius of the straw-cleaning wheel, mm; h is the working depth of the row cleaner, mm; α is the angle between the straw-cleaning wheel and the forward direction, ($^\circ$); and β is the angle between the straw-cleaning wheel and the vertical plane, ($^\circ$).

As seen in Equation (2), when the parameters of the row cleaner were determined, the working breadth B only correlated with the working depth h , and the automatic-width control system was developed based on this. The system regulated the working depth by monitoring the soil downforce of the straw-cleaning wheels in real time to ensure the stability of the working width. The schematic diagram of the main hardware in the system is illustrated in Figure 7. Specifically, the U1 was a microcontroller consisting of an STM32F103ZET6 Single-Chip Microcomputer (SCM); the P1 was an S-shaped pressure sensor, in which the signal output terminals S+ and S- were, respectively, connected through a transduction amplifier to the ADC input pins, the PA1 and PA2 of the SCM. K1 and K2 were two peckers of the same type and function to control the stretching transformation of the electric linear actuator. The control ends of K1 and K2 were connected to the I/O pins PG6 and PG7 of the SCM, respectively, and their joint end was connected to two signal lines of the electric linear actuator, and the normal closed end was linked to the 24 V power supply. The normal open end was grounded. When the pin PG6 was at a high level and the pin PG7 outputted a low-level current, the electric linear actuator elongated; otherwise, the electric linear actuator contracted. When PG6 and PG7 were at the same level (either at a high or low level), the electric linear actuator did not move. Both S1 and S2 were the key modules, and U2 was the liquid crystal display (LCD) module, which realized the function of human-computer interaction.

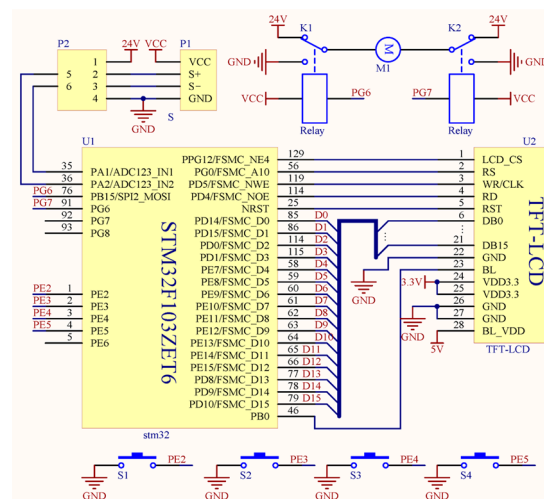


Figure 7. The main hardware design circuit of the automatic-width control system.

The system control flow is shown in Figure 8. When the system started to work, the internal resources were initialized first, including the system clock, I/O port, relevant registers, etc. The conversion parameter between the working width of the row cleaner and the output value from the S-shaped pressure sensor were stored in an array. Then, the SCM read the A/D switching value, V_{ad} , outputted from the S-shaped pressure sensor, and converted V_{ad} to the corresponding working width value which was B_t according to the conversion parameter as stored. The B_t at this moment was the real-time-detected working width. If B_t surpassed the preset working width threshold B_0 , the SCM estimated the corresponding difference ΔB ($\Delta B = B_t - B_0$) and thereby controlled the electric linear actuator to contract accordingly, so the row cleaner returned to the preset working width. On the contrary, if B_t was smaller than B_0 , the electric linear actuator elongated by the corresponding stroke, so the row cleaner returned to the preset working width. Relevant information (e.g., preset width B_0 , detected width B_t) was displayed on the LCD.

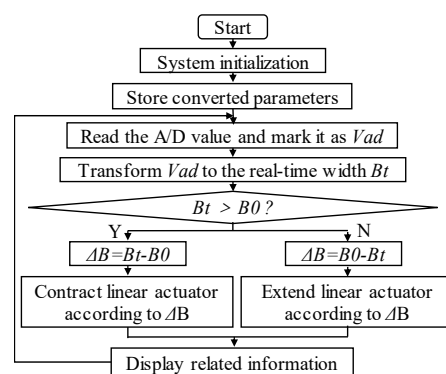


Figure 8. Automatic-width control system workflow.

2.2.4. Design of Tillage-Depth-Stabilization Control System

The tillage-depth-stabilization control system applies variable downforce to the parallel four-bar profiling mechanism of the row unit. In addition, it adjusts the internal pressure of the air spring through an electric proportional valve to achieve real-time and precise control of the downforce of the row unit on the ground, thereby improving the working depth stability. As shown in Figure 9, the system mainly consisted of a control module and a pneumatic transmission actuator. The control module consisted of a single chip microcomputer (SCM), a D/A converter, a voltage amplifier, a liquid crystal display (LCD), and a key-press array. The pressure transmission actuator consisted of an air compressor, a gas tank, an air pressure sensor, a filter, an electric-pneumatic regulator, and an air spring.

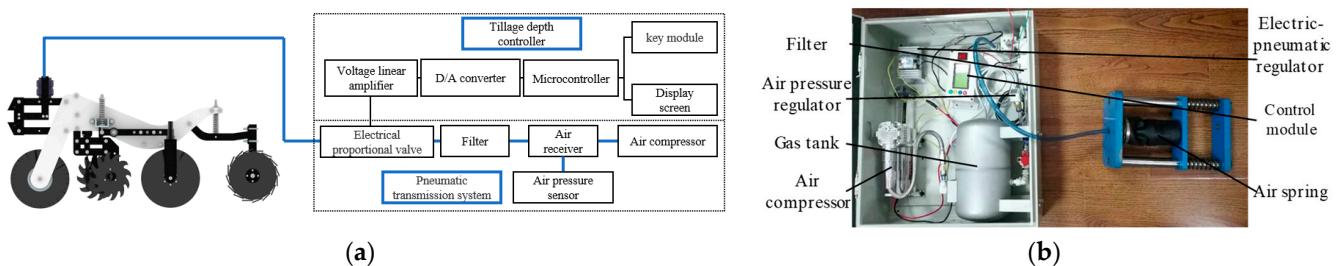


Figure 9. Tillage-depth stabilization system: (a) schematic diagram; (b) an image of the system.

The control module was used to monitor pressure changes inside the air spring, and controlled tillage depth stability through real-time adjustment of gas flows by the electric-pneumatic regulator. The schematic diagram of the main hardware in the system is illustrated in Figure 10. This control module adopted a D/A converter (TLC5615 chips) to convert analog/digital signals, and used an STC12C5A60S2 Single-Chip Microcomputer as the microprocessor. The SMC ITV3050-312 electric-pneumatic regulator was inputted with

0–10 V analog/voltage signals. The ISOEM-U1-P2-O5 voltage amplifier can realize a double-gain function to the output signals from the SCM. The analog-to-digital converter ADC4 integrated in the SCM was used as the pins of the electric-pneumatic regulator to collect the internal pressures of the air spring. The port P0 was used as the data communication interface of the LCD module. The I/O pins P2.0–P2.1 simulated the IIC communication outlets, so as to ensure communication between the SCM and the D/A converter. The voltage regulator chip TL431 offered a basic reference voltage to the D/A converter, which ensured its working stability. The four buttons of the key-press array were connected via a low-level triggering mode to the I/O pins P3.4, P3.5, P3.6, and P3.7 of the SCM, respectively.

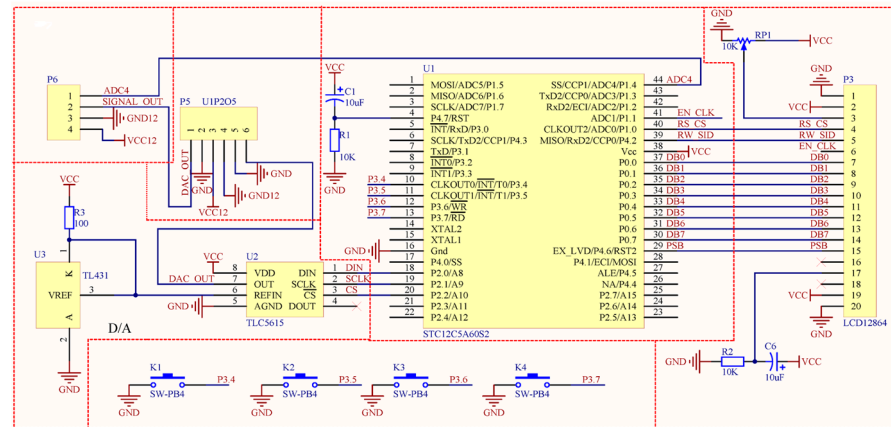


Figure 10. The main hardware design circuit of the tillage-depth-stabilization control system.

The pneumatic transmission actuator provided enough usable air pressure to adjust the intrinsic pressure stability of the air spring. The work flow is shown in Figure 11. Firstly, the D/A converter, LCD screen, ADC, I/O port, and relevant registers of the system were initialized. Then, the SCM waited to receive a target value of pressure from the user through the button module. After the SCM received the target pressure, it converted the pressure to a digital voltage signal according to the linear relationship between the pressure and the input control of the electric-pneumatic regulator. The digital voltage signal outputted from the SCM can be converted by the D/A converter to an analog voltage signal. When the analog voltage signal was outputted from the D/A converter, the system software operated the ADC program and collected the real-time internal air pressures of the air spring, which were displayed on the LCD. Hence, the analog voltage signal from the D/A converter was amplified in the linear gain by the voltage amplifier and then acted on the electric-pneumatic regulator. After that, the internal pressures of the air spring were automatically regulated to be constant via the proportional valve. Finally, the tillage depth stability was maintained.

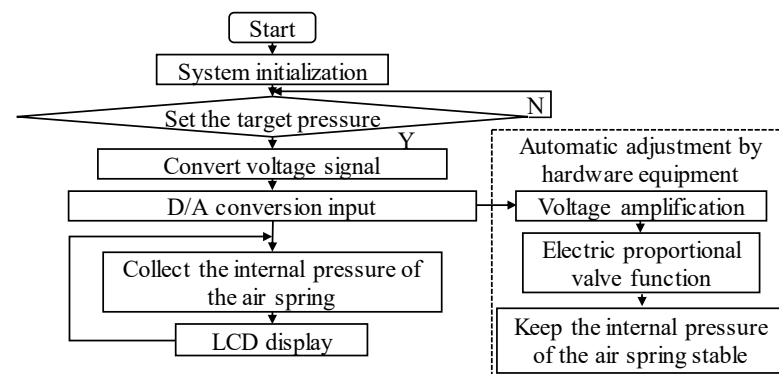


Figure 11. Tillage-depth-stabilization control system workflow.

2.3. Field Test

2.3.1. Test Preparation

The field test was conducted at the agriculture experiment field (43.84° N, 125.33° E; altitude 228 m) of Jilin University, Changchun, Jilin province. The soil in the field belonged to the typical black clay of Northeastern China. The study site was a corn stubble field; the aboveground corn straws were crushed by a combine harvester and evenly covered the soil surface. The daily average air temperature was 12–16 °C and no precipitation occurred during the tests. The main parameters are shown in Table 3.

Table 3. Main parameters of field tests.

Parameters		Values
Straw residue	Line spacing/mm	650
	Plant spacing/mm	220
	Residue length/mm	50–150
	Stubble height/mm	50–100
	Weight of residue/kg·m ⁻²	1.4
	Moisture content/%	50
0–100 mm Soil layer	Soil cone index/MPa	0.985
	Moisture content/%	24.6
	Bulk density/g·cm ⁻³	1.21
	Temperature/°C	11.8

The machine tested was supplied with traction by a John Deere 704-type tractor, and the machine's automatic control system was supplied with power from the tractor's electric battery. The test site and working situation are shown in Figure 12.



Figure 12. Test site and working situation.

2.3.2. Test Contents

Tests were conducted to assess the operational performance and adaptivity of the automatic strip-till machine. Each test plot was 3 m wide and 120 m long, and consisted of one 10 m adjusting zone at each end, and a stable 100 m data acquisition zone in the middle. The tests were designed as a single factor test, and the test factors included 5 internal pressures of the air spring (0.3 Mpa, 0.4 Mpa, 0.5 Mpa, 0.6 Mpa, and 0.7 Mpa), 5 theoretical working widths (18 cm, 20 cm, 22 cm, 24 cm, and 26 cm), and 5 working speeds (6 km/h, 8 km/h, 10 km/h, 12 km/h, and 14 km/h). Each group was conducted 3 times, and the calculated average values were used as the test results.

2.3.3. Test Indexes

The measurements were carried out in accordance with the Chinese National Standard GB/T 24675.1-2009.

(1) Tillage depth and tillage depth stability coefficient (D , S_D)

After each operation, the starting site in a test plot was randomly selected, and along the advancing direction of the machine, 20 measuring points were consecutively detected at an interval of 2 m. The D and S_D was calculated as follows:

$$a_j = \frac{\sum_{i=1}^{n_j} a_{ji}}{n_j} \quad (3)$$

$$S_j = \sqrt{\frac{\sum_{i=1}^{n_j} (a_{ji} - a_j)^2}{n_j - 1}} \quad (4)$$

$$S_{Dj} = \left(1 - \frac{S_j}{a_j}\right) \times 100\% \quad (5)$$

where a_j is the average tillage depth of the j -th running, cm; a_{ji} is the tillage depth at point i in the j -th running, cm; n_j is the number of measuring points in the j -th running; S_j is the tillage depth standard deviation in the j -th running, cm; and S_{Dj} is the tillage depth stability coefficient of the j -th running.

(2) Working width and width stability coefficient (W , S_W)

The measurement and calculation of W and S_W are the same as those of D and S_D .

(3) Furrow bottom roughness and soil surface roughness (R_B , R_S)

A self-designed furrow profile meter was used to measure the furrow bottom roughness and soil surface roughness after operation. Furrow bottom and soil surface profiles were plotted on coordinate papers, and the difference between the maximum and minimum was calculated as the R_B and R_S .

(4) Straw cleaning rate (C)

A total of 10 consecutive measuring points were set at an interval of 2 m in the stable operation zone. The residual straw within the measurement area (25 cm wide, 100 cm long) was weighed on an electronic balance. The ratio to the straw weight before and after each test was calculated, and the average value was C .

(5) Soil breakage rate (G_S)

In each row, 1 point was measured, and samples were collected along the working direction. The weight of each soil mass with the largest edge length < 4 cm inside the plow layer and the total soil were weighed. The test zone was 25 cm wide and 100 cm long. The G_S is the ratio of the two weight values.

2.3.4. Statistical Analyses

Analysis of variance (ANOVA) was used to analyze the variance in the obtained data. Means were compared using the Least Significant Difference (LSD) test.

3. Results and Discussion

The analysis of variance of the variables, with the respective means, levels, and results of the F-tests, is shown in Table 4.

Table 4. Test results.

Factors	Variables							
	C/%	D/cm	S _D /%	W/cm	S _W /%	R _B /cm	R _S /cm	G _S /%
Pressures, F1 (the speed was 10 km/h, and the tillage width was 22 cm)								
0.3 Mpa (P1)	92.4 ± 0.29 a	5.7 ± 0.23 e	93.7 ± 0.12 a	22.4 ± 0.06 d	94.5 ± 0.12 a	1.2 ± 0.12 b	1.3 ± 0.12 b	94.5 ± 0.23 b
0.4 Mpa (P2)	92.3 ± 0.17 a	8.2 ± 0.12 d	93.3 ± 0.12 ab	22.4 ± 0.17 d	93.1 ± 0.40 a	1.2 ± 0.06 b	1.5 ± 0.12 b	94.3 ± 0.29 b
0.5 Mpa (P3)	92.0 ± 0.29 a	10.5 ± 0.12 c	93.3 ± 0.23 b	22.7 ± 0.12 c	92.5 ± 0.40 b	1.6 ± 0.12 b	1.6 ± 0.17 b	95.7 ± 0.35 a
0.6 Mpa (P4)	91.7 ± 0.23 a	12.3 ± 0.23 b	92.3 ± 0.35 b	23.4 ± 0.17 b	91.5 ± 0.58 bc	2.2 ± 0.40 a	2.3 ± 0.23 a	91.7 ± 0.35 c
0.7 Mpa (P5)	91.9 ± 0.35 a	13.5 ± 0.17 a	91.7 ± 0.92 b	24.3 ± 0.29 a	89.7 ± 0.98 c	2.8 ± 0.23 a	2.7 ± 0.17 a	89.3 ± 0.46 d
Speed, F2 (the tillage depth was 10 cm, and the tillage width was 22 cm)								
6 km/h (V1)	91.2 ± 0.46 b	10.3 ± 0.12 a	93.40 ± 0.92 ab	22.4 ± 0.06 c	95.3 ± 0.92 a	1.5 ± 0.06 c	1.7 ± 0.06 a	92.4 ± 0.35 c
8 km/h (V2)	92.3 ± 0.46 ab	10.5 ± 0.12 a	94.70 ± 0.58 a	22.0 ± 0.23 c	93.4 ± 0.23 b	1.8 ± 0.29 c	1.4 ± 0.12 b	93.2 ± 0.17 b
10 km/h (V3)	92.4 ± 0.35 ab	10.2 ± 0.23 a	94.30 ± 0.75 a	22.3 ± 0.17 c	92.1 ± 0.29 bc	1.6 ± 0.12 c	1.5 ± 0.06 ab	94.9 ± 0.12 a
12 km/h (V4)	93.6 ± 0.06 a	10.0 ± 0.46 ab	92.10 ± 1.39 ab	23.9 ± 0.29 b	90.9 ± 0.52 c	1.7 ± 0.12 b	1.4 ± 0.12 b	95.3 ± 0.35 a
14 km/h (V5)	92.1 ± 0.75 b	9.40 ± 0.12 b	90.90 ± 0.06 b	25.6 ± 0.17 a	88.7 ± 0.40 d	1.8 ± 0.23 a	1.5 ± 0.06 ab	95.6 ± 0.12 a
Tillage width, F3 (the tillage depth was 10 cm, and the speed was 10 km/h)								
18 cm (WT1)	92.9 ± 0.26 a	10.2 ± 0.06 a	95.2 ± 0.58 a	18.9 ± 0.23 e	93.6 ± 0.64 a	1.1 ± 0.12 c	0.8 ± 0.06 d	96.6 ± 0.23 a
20 cm (WT2)	91.5 ± 0.40 b	10.1 ± 0.12 ab	94.7 ± 0.58 a	21.1 ± 0.29 d	92.1 ± 0.40 ab	1.2 ± 0.12 bc	1.3 ± 0.12 c	94.8 ± 0.29 b
22 cm (WT3)	92.0 ± 0.58 ab	10.2 ± 0.12 b	93.4 ± 1.15 ab	22.4 ± 0.29 c	92.5 ± 0.58 ab	1.6 ± 0.17 b	1.5 ± 0.17 c	95.2 ± 0.23 b
24 cm (WT4)	93.3 ± 0.46 a	10.1 ± 0.12 ab	92.7 ± 1.15 ab	24.5 ± 0.35 b	91.9 ± 0.46 b	2.2 ± 0.12 a	2.4 ± 0.12 b	92.4 ± 0.40 c
26 cm (WT5)	92.7 ± 0.35 ab	9.80 ± 0.17 b	91.2 ± 1.15 b	26.3 ± 0.17 a	93.3 ± 0.35 ab	2.6 ± 0.17 a	2.8 ± 0.12 a	89.8 ± 0.40 d
F-test								
F1	ns	**	ns	*	*	*	*	**
F2	ns	ns	ns	**	**	ns	ns	**
F3	ns	ns	ns	**	ns	**	**	**

The data consist of mean and standard error. Data followed by the same letter in the column do not differ significantly when using the LSD test ($p < 0.05$). ** indicates extremely significant ($p < 0.01$), * indicates significant ($p < 0.05$), and ns indicates insignificant ($p > 0.05$).

3.1. Effects of Internal Pressure of Air Spring on Working Performance

It can be seen from Table 4 that the internal pressure of the air spring significantly affected the tillage depth (D), width (W), width stability (S_W), furrow bottom roughness (R_B), surface roughness (R_S), and soil breakage rate (G_S), but did not significantly affect the straw cleaning rate (C) or tillage depth stability (S_D).

As shown in Figure 13, with the rise in the internal pressure of the air spring, the tillage depth (D), width (W), furrow bottom roughness (R_B), and surface roughness (R_S) all increased, but the width stability (S_W) and soil breakage rate (G_S) both declined. At the internal pressure of 0.7 MPa, the soil breakage rate (G_S) and width stability dropped by 89.3% and 89.7%, respectively, and the surface roughness and bottom roughness increased to 2.8 cm and 2.7 cm, respectively. The reason for this was that the excessive internal pressure of the air spring increased the tillage depth of the machine, which increased the amount of soil loosening and soil moisture, but led to a weakening in the effect of the coulters on the soil and a reduction in the working quality of the machine. This is similar to Zbigniew Kogut’s findings that the deeper the disc harrow operates, the greater the working resistance, including traction and vertical force [30]. P. Balsari et al. reached similar conclusions in their study of a tractor-powered harrow [31]. Hence, the applicable internal pressure of the air spring for this machine was 0.3–0.6 MPa.

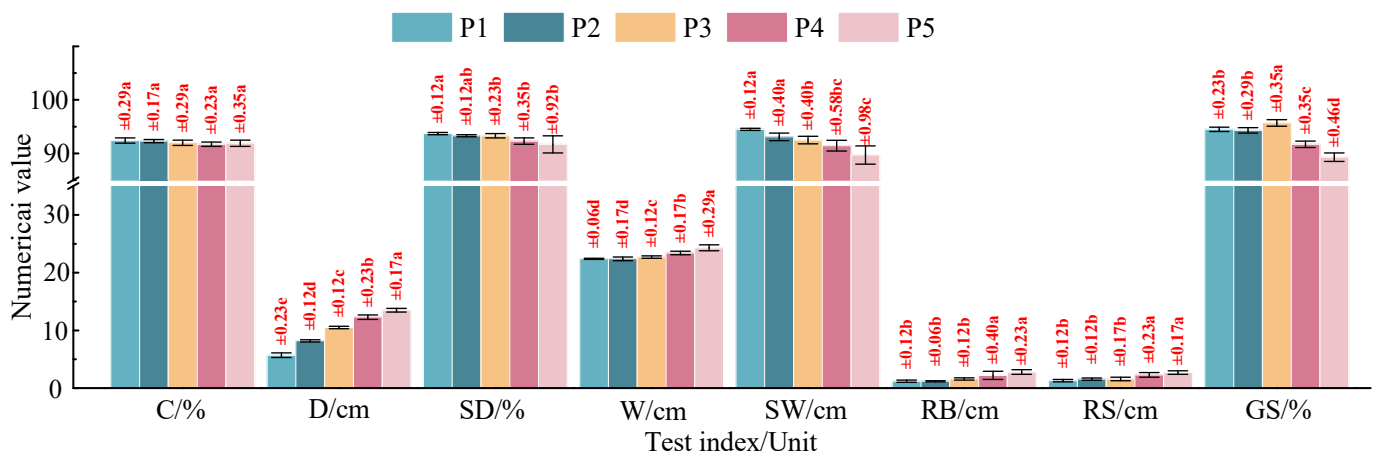


Figure 13. Effects of the internal pressure of the air spring on working performance: error bars are standard deviations, values are standard errors, and means followed by different lowercase letters are significantly different according to the LSD multiple range test at a significance level of 0.05.

In order to obtain the corresponding relationship between the internal pressure of the air spring and tillage depth, a regression analysis was performed. The regression equation of the quadratic polynomial simulation model is:

$$y = 0.0028x^2 - 0.004x + 0.2351 \tag{6}$$

The actual corresponding relationship between tillage depth and internal pressure of the air spring was obtained according to Equation (6), as shown in Table 5.

Table 5. The corresponding relationship between tillage depth and internal pressure of the air spring.

Index	Corresponding Value			
Tillage depth/cm	6	8	10	12
Internal pressure of air spring/MPa	0.35	0.40	0.49	0.61

3.2. Effects of Working Speed on Working Performance

As can be seen from Table 4, the working speed significantly affected the width (W), width stability (S_W), and soil breakage rate (G_S), but did not significantly affect the cleaning rate (C), tillage depth (D), tillage depth stability (S_D), surface roughness (R_S), or furrow bottom roughness (R_B).

As shown in Figure 14, with the rise in working speed, the width (W) and soil breakage rate (G_S) both increased, but the width stability (S_W) declined. At the working speed of 14 km/h, the width (W) rose to 25.6 cm, and the width stability (S_W) declined to 88.7% (Table 4). The reason for this was that the increase in the working speed increased the rotation speed of all rotating working parts, and enhanced the interaction between the coulters and the soil, which intensified the breakage and throwing of soil. Hence, when the throwing occurred at too high a speed, this led to an increase in the tilling width and soil breakage rate and to a decline in width stability. This is similar to the research results of Zeng and Chen: when two types of fluted coulters were working at high speed in wheat fields, the width of the furrow significantly increased with the increase in working speed, and it is believed that the effect of working speed was more dominant than the coulters geometry on the tillage performance of the fluted coulters [32]. James B. Barr also pointed out that, as the working speed increased, so did the soil disturbance and lateral soil throw of the opener [33]. Thus, the applicable working speed of this machine was 6–12 km/h.

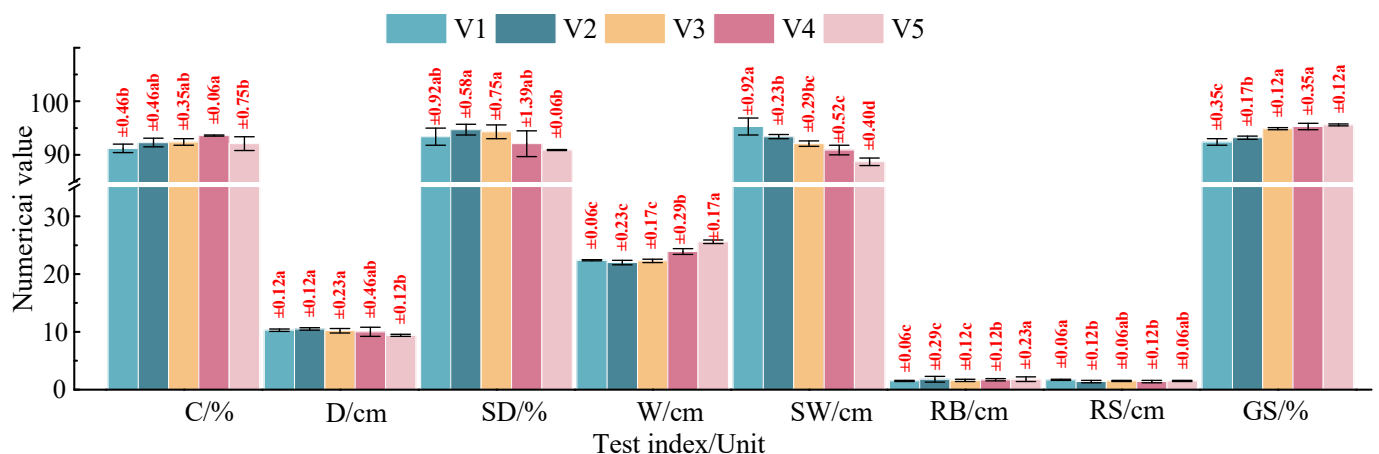


Figure 14. Effects of working speed on working performance: error bars are standard deviations, values are standard errors, and means followed by different lowercase letters are significantly different according to the LSD multiple range test at the significance level of 0.05.

3.3. Effects of Theoretical Tillage Width on Working Performance

As can be seen from Table 4, the theoretical tillage width significantly affected the width (W), furrow bottom roughness (R_B), surface roughness (R_S), and soil breakage rate (G_S), but did not significantly affect the cleaning rate (C), tillage depth (D), tillage depth stability (S_D), or width stability (S_W).

As shown in Figure 15, with the rise in theoretical tillage width, the width (W), furrow bottom roughness (R_B), and surface roughness (R_S) all increased, but the soil breakage rate (G_S) declined. At the theoretical tillage width of 26 cm, the soil breakage rate of this machine declined to 89.8%, and the furrow bottom roughness and surface roughness rose to 2.6 and 2.8 cm, respectively. The reasons were that too large a tillage width gradually enlarged the distance between the two symmetrical coulters of the profiling soil-loosening device, so that the thrown and collision effects of the loose soil between the coulters were weakened. Moreover, too large a distance surpassed the soil disturbance width of single coulters, and so the soil breakage rate, furrow bottom roughness, and surface roughness all declined. This is similar to Hang's finding that undisturbed soil increases through increasing the spacing between two V-shaped subsoiling tines [34]. Hence, the applicable theoretical tillage width for this machine was 18–24 cm.

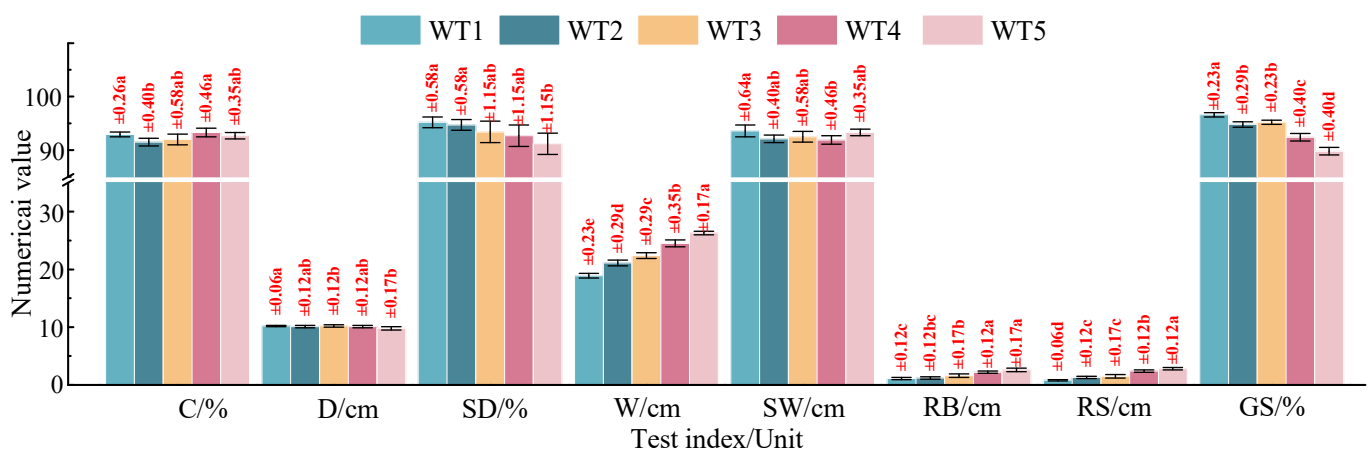


Figure 15. Effects of theoretical tillage width on working performance: error bars are standard deviations, values are standard errors, and means followed by different lowercase letters are significantly different according to the LSD multiple range test at the significance level of 0.05.

4. Conclusions

In this study, an automatic strip-till machine was designed. The conventional corn planting model in Northeastern China was analyzed, and the main structure and working parameters of the machine were determined. An automatic control system was developed to improve the operational stability of the machine. The applicable range of the machine was determined through field tests. The following conclusions were obtained:

- (1) The operating process of the machine was identified as straw cutting > straw cleaning > soil loosening > soil crushing, and the machine could complete the construction of high-quality seedbeds under straw mulching in one session.
- (2) The coulters for straw cutting and soil loosening were identified to be 18 w and 13 w by analyzing the field test results. The key parameters of the V-shaped crushing wheel were determined, the crushing wheel radius was 165 mm, and the number of soil-crushing teeth evenly distributed on the circumference was 16. Based on a pressure sensor and an electric linear actuator, an automatic-width-control row cleaner was designed, which could realize the real-time monitoring and control of the soil downforce and working depth of the straw-cleaning wheels to enhance the width stability of the cleaning devices. A tillage-depth-stabilization control system was designed, which used an air spring as the downforce source. An electric proportional valve was used to monitor and regulate the internal pressure of the air spring, so that the downforce of the row unit could be precisely adjusted.
- (3) The field test results showed that when the forward speed, tillage depth, and theoretical width were 6–12 km/h, 6–12 cm, and 18–24 cm, respectively, the straw cleaning rate, soil crushing rate, and tillage depth and breadth stability were higher than 90%, and the soil flatness was less than 2 cm. The land condition after the operation of the machine met the agronomic and technical requirements for corn planting.
- (4) There is a limitation to the findings of this paper. The test results were obtained in a defined plot, so the machine may need to be made adjustable when used in other plots. In future studies, the machine will be evaluated in the field using farm-scale equipment.

Author Contributions: Conceptualization, Q.W.; methodology, Q.W.; software, Q.W.; validation, B.W. and M.S.; formal analysis, Q.W. and B.W.; investigation, Q.W. and H.T.; resources, Q.W.; data curation, Q.W. and M.S.; writing—original draft preparation, Q.W.; writing—review and editing, B.W. and M.S.; visualization, J.W., X.S. and W.Z.; supervision, J.W.; project administration, J.W.; funding acquisition, Q.W. and J.W. All authors have read and agreed to the published version of the manuscript.

Funding: This research was financially supported by the National Natural Science Foundation of China (No. 52005094), the Heilongjiang Provincial Natural Science Foundation of China (No. LH2022E006), the Heilongjiang Provincial Key Research and Development Program (No. 2022ZX05B04, No. 2022ZX05B05), the Heilongjiang Postdoctoral Foundation (No. LBH-Z19041), and the Scholars Program of Northeast Agricultural University (No. 20QC10).

Institutional Review Board Statement: Not applicable.

Data Availability Statement: Not applicable.

Acknowledgments: The authors would like to thank their schools and colleges, as well as the funding providers of the project. All support and assistance are sincerely appreciated.

Conflicts of Interest: The authors declare no conflict of interest.

References

- Ahmad, F.; Adeel, M.; Qiu, B.J.; Ma, J.; Shoaib, M.; Aamir, S.; Chandio, F.A. Sowing uniformity of bed-type pneumatic maize planter at various seedbed preparation levels and machine travel speeds. *Int. J. Agric. Biol. Eng.* **2021**, *14*, 165–171. [[CrossRef](#)]
- Yang, S. Status and Trends of Maize Industry Development in Northeast China. *China Seed Ind.* **2015**, *4*, 6–8.
- Ou, Y.; Rousseau, A.N.; Wang, L.; Yan, B. Spatio-temporal patterns of soil organic carbon and pH in relation to environmental factors—A case study of the Black Soil Region of Northeastern China. *Agric. Ecosyst. Environ.* **2017**, *245*, 22–31. [[CrossRef](#)]
- Han, X.Z.; Zou, W.X. Effects and Suggestions of Black Soil Protection and Soil Fertility Increase in Northeast China. *Bull. Chin. Acad. Sci.* **2018**, *33*, 206–212.
- Zhao, H.; Zheng, Y.T.; Lü, Y.Z.; Yuan, L.W.; Zeng, X.N. The difference of black soil humus content and structure in no-tillage and plowing tillage. *Ecol. Environ. Sci.* **2010**, *19*, 1238–1241.
- Hu, H.N.; Li, H.W.; Wang, Q.J.; He, J.; Lu, C.Y.; Wang, Y.B.; Liu, P. Anti-blocking performance of ultrahigh-pressure waterjet assisted furrow opener for no-till seeder. *Int. J. Agric. Biol. Eng.* **2020**, *13*, 64–70. [[CrossRef](#)]
- Muresan, A.O.; Indrea, D.; Maniutiu, D.; Sima, R. The effect of minimum strip-tillage cover crop system on a few vegetable crops. *J. Hortic. For. Biotechnol.* **2011**, *15*, 35–39.
- Shittu, K.A.; Adeboye, O.B.; Oyedele, D.J.; Lamidi, W.A.; Babatunde, M.K.; Mosobalaje, A.-S.M. Impact of Tillage Practices on properties of Soil, Evapotranspiration and Productivity of Cowpea in Nigeria. *Trop. Subtrop. Agroecosyst.* **2023**, *26*, #030. [[CrossRef](#)]
- Weener, B.R.; Osbome, S.L.; Lehman, R.M.; Kumar, S. Seven-year impact of cover crops on soil health when com residue is removed. *BioEnergy Res.* **2018**, *11*, 239–248.
- Liu, Z.; Gu, H.; Liang, A.; Li, L.; Yao, Q.; Xu, Y.; Liu, J.; Jin, J.; Liu, X.; Wang, G. Conservation tillage regulates the assembly, network structure and ecological function of the soil bacterial community in black soils. *Plant Soil* **2022**, *472*, 207–223. [[CrossRef](#)]
- He, J.; Li, H.W.; Chen, H.T.; Lu, C.Y.; Wang, Q.J. Research Progress of Conservation Tillage Technology and Machine. *Trans. Chin. Soc. Agric. Mach.* **2018**, *49*, 1–19.
- Zhao, J.L.; Guo, M.Z.; Lu, Y.; Huang, D.Y.; Zhuang, J. Design of bionic locust mouthparts stubble cutting device. *Int. J. Agric. Biol. Eng.* **2020**, *13*, 20–28. [[CrossRef](#)]
- Liu, P.; He, J.; Li, H.; Wang, Q.; Lu, C.; Zheng, K.; Liu, W.; Zhao, H.; Lou, S. Effect of straw retention on crop yield, soil properties, water use efficiency and greenhouse gas emission in China: A meta-analysis. *Int. J. Plant Prod.* **2019**, *13*, 347–367. [[CrossRef](#)]
- Jia, H.L.; Wang, Q.; Huang, D.Y.; Zhu, L.T.; Li, M.W.; Zhao, J.L. Design of bionic mole forelimb intelligent row cleaners. *Int. J. Agric. Biol. Eng.* **2019**, *12*, 27–35. [[CrossRef](#)]
- Al-kaisi, M.; Hanna, H.M. *Resource Conservation Practices: Consider the Strip-Tilling Alternative*; Iowa State University: Ames, IA, USA, 2008.
- Tillman, J.; Nair, A.; Gleason, M.; Batzer, J. Evaluating strip tillage and rowcover use in organic and conventional muskmelon production. *Horttechnology* **2015**, *25*, 487–495. [[CrossRef](#)]
- Townsend, T.J.; Ramsden, S.J.; Wilson, P. How do we cultivate in England? Tillage practices in crop production systems. *Soil Use Manag.* **2016**, *32*, 106–117. [[CrossRef](#)] [[PubMed](#)]
- Celik, A.; Altikat, S.; Way, T.R. Strip tillage width effects on sunflower seed emergence and yield. *Soil Tillage Res.* **2013**, *131*, 20–27. [[CrossRef](#)]
- Godsey, C.; Kochenower, R.; Taylor, R. *Strip-Till Considerations in Oklahoma*; Oklahoma Cooperative Extension Service: Stillwater, OK, USA, 2007.
- Alghamdi, R.S.; Daigh, A.L.M.; DeJong-Hughes, J.; Wick, A.F. Soil temperature and water contents among vertical tillage, strip tillage, and chisel plowing in the Upper Great Plains. *Can. J. Soil Sci.* **2021**, *101*, 596–616. [[CrossRef](#)]
- Jaskulska, I.; Romanekas, K.; Jaskulski, D.; Gałezewski, L.; Breza-Boruta, B.; Dębska, B.; Lemanowicz, J. Soil properties after eight years of the use of strip-till one-pass technology. *Agronomy* **2020**, *10*, 1596. [[CrossRef](#)]
- Laufer, D.; Koch, H.J. Growth and yield formation of sugar beet (*Beta vulgaris* L.) under strip tillage compared to full width tillage on silt loam soil in Central Europe. *Eur. J. Agron.* **2017**, *82*, 182–189. [[CrossRef](#)]

23. Evans, R.G.; Stevens, W.B.; Iversen, W.M. Development of Strip Tillage on Sprinkler Irrigated Sugarbeet. *Appl. Eng. Agric.* **2010**, *26*, 59–69. [[CrossRef](#)]
24. Wolkowski, R.P. Row-placed fertilizer for maize grown with an in-row crop residue management system in southern Wisconsin. *Soil Tillage Res.* **2000**, *54*, 55–62. [[CrossRef](#)]
25. Sorensen, B. *A Comparison of Soil Properties and Plant-to-Plant Variability in No-Till and Strip-Till Corn Fields in Illinois*; University of Illinois at Urbana-Champaign: Champaign, IL, USA, 2014.
26. Vyn, T.J.; Raimbault, B.A. Evaluation of strip tillage systems for corn production in Ontario. *Soil Tillage Res.* **1992**, *23*, 163–176. [[CrossRef](#)]
27. Jia, H.L.; Wang, G.; Jiang, T.J.; Liu, H.; Zhuang, W.L. Design and Experiment of 1GH-3 Inter-row Tillage Machine. *Trans. Chin. Soc. Agric. Mach.* **2012**, *43*, 35–41&160.
28. Wang, Q.; Zhu, L.T.; Li, M.W.; Huang, D.Y.; Jia, H.L. Conservation Agriculture Using Coulters: Effects of Crop Residue on Working Performance. *Sustainability* **2018**, *10*, 4099. [[CrossRef](#)]
29. Wang, Q.; Jia, H.L.; Zhu, L.T.; Li, M.W.; Zhao, J.L. Design and Experiment of Star-toothed Concave Disk Row Cleaners for No-till Planter. *Trans. Chin. Soc. Agric. Mach.* **2019**, *50*, 68–77.
30. Kogut, Z.; Sergiel, L.; Zurek, G. The effect of the disc setup angles and working depth on disc harrow working resistance. *Biosyst. Eng.* **2016**, *151*, 328–337. [[CrossRef](#)]
31. Balsari, P.; Biglia, A.; Comba, L.; Sacco, D.; Alcatrao, L.E.; Varani, M.; Mattetti, M.; Barge, P.; Tortia, C.; Manzone, M.; et al. Performance analysis of a tractor- power harrow system under different working conditions. *Biosyst. Eng.* **2021**, *202*, 28–41. [[CrossRef](#)]
32. Zeng, Z.W.; Chen, Y. The performance of a fluted coulters for vertical tillage, as affected by working speed. *Soil Tillage Res.* **2018**, *175*, 112–118. [[CrossRef](#)]
33. Barr, J.B.; Desbiolles, J.M.A.; Fielke, J.M.; Ucgul, M. Development and field evaluation of a high-speed no-till seeding system. *Soil Tillage Res.* **2019**, *194*, 104337. [[CrossRef](#)]
34. Hang, C.G.; Gao, X.J.; Yuan, M.C.; Huang, Y.X.; Zhu, R.X. Discrete element simulations and experiments of soil disturbance as affected by the tine spacing of subsoiler. *Biosyst. Eng.* **2018**, *168*, 73–82. [[CrossRef](#)]

Disclaimer/Publisher’s Note: The statements, opinions and data contained in all publications are solely those of the individual author(s) and contributor(s) and not of MDPI and/or the editor(s). MDPI and/or the editor(s) disclaim responsibility for any injury to people or property resulting from any ideas, methods, instructions or products referred to in the content.